Lithium Niobate Optomechanical Disk Resonators

Renyuan Wang
FAST Labs™, BAE Systems
Nashua, New Hampshire, USA
renyuan.wang@baesystems.com

Sunil A. Bhave
OxideMEMS Lab, Purdue University
West Lafayette, Indiana, USA
bhave@purdue.edu

***Abstract*— Lithium Niobate (LN or just niobate) thin-film micro-photonic resonators have promising prospects in many applications including high efficiency electro-optic modulators, opto-mechanics and nonlinear optics. This paper presents free-standing thin-film lithium niobate optomechanical resonators on a silicon platform using MEMS fabrication technology. We fabricated a 35 micron radiu niobate disk resonator that exhibits high intrinsic optical quality factor (Q) of 484,000. Exploiting the optomechanical interaction from the released free-standing structure and high optical Q, we were able to demonstrate acousto-optic modulation from these devices by exciting the 56 MHz radial breathing mode (mechanical Q of 2700) and 1.9 GHz mechanical mode using a hovering probe.**

Keywords— Micromachining, Lithium Niobate, optomechanics disk resonator, acousto-optic modulator

I. INTRODUCTION

The lack of inversion symmetry in the Lithium Niobate (LN or niobate) crystal exhibits itself via its characteristic strong piezoelectric effect, linear electro-optic effect, pyroelectric effect and strong second order optical nonlinearity [1]. Since our first demonstration of free-standing lithium niobate optical resonator and its optomechanical interactions [2], the non-linear photonics and optomechanics communities have embraced the power and demonstrated capabilities in non-linear photonics, electro-optic modulation [3], chip-scale frequency combs [4], acousto-optic gyroscopes [5] and acousto-optic modulation for ultra-low V_{pi} microwave-to-optical conversion[6,7]. Most demonstrations involve a suspended membrane or timed-undercut, with a wedge-like etch cross-section to achieve excellent optical performance. In this paper we report on a center-pedestal supported niobate disk resonator achieving acousto-optical modulation up to 1.9 GHz.

Microring resonators and microdisk resonators are fundamental building blocks for many micro-photonic devices including filters [10], lasers [11], and modulators [9]. A high Q thin-film $LiNbO_3$ resonator has the potential to enable many novel and high performance devices. While anisotropic etching defined thin-film $LiNbO_3$ photonic structures are desired for applications such as photonic crystals and resonators, the Q demonstrated to date from such devices is generally limited to few thousand, while the quality factor from bulk $LiNbO_3$ disk resonators can exceed 10^8 [8]. The key limiting factor of the quality factor is the optical scattering loss from the rough side wall profile from the etching process. Surface smoothing by heating the device close to the melting point of $LiNbO_3$ has been attempted [12] with limited success ($Q\sim3\times10^4$). In [6], the optical Q is improved to 7.2×10^4 by etching a deposited cladding layer of slab waveguides with the drawback of reduced optical confinement. [13] has demonstrated a $LiNbO_3$ thin-film fabrication technology for manufacturing free-standing LiNbO3 RF MEMS devices, where we were able to achieve smooth and nearly vertical etching profile of $LiNbO_3$ using a ion mill etching process on a full 4 inch 1um thick $LiNbO_3$ thin-film on $LiNbO_3$ substrate wafer. In contrast to focused ion beam etching, our process uses a uniform broad argon ion beam, and is batch fabrication compatible. Leveraging these MEMS fabrication techniques, we demonstrate here free-standing thin-film $LiNbO_3$ microdisk resonator on silicon substrate with one of the highest optical Q. Moreover, the free-standing structure allows the coupling between the mechanical domain and optical domain, with which we also demonstrate acousto-optic modulation from the resonator.

II. DEVICE FABRICATION

There are three distinct fabrication challenges to fabricate the LN micro-photonic resonator on silicon substrate: 1. Achieving $LiNbO_3$ thin-film with bulk single crystal $LiNbO_3$ quality, 2. Achieving vertical side-wall and smooth surface profiles without mask residue, 3. Achieving clearance between the LN device and silicon substrate to enable efficient mode confinement.

The common technique for fabricating $LiNbO_3$ thin-film is by ion-slicing [14]. The drawback is that this process requires an annealing step to recover the crystal quality from the damage caused by the ion implantation. The annealing process unavoidably cause thermal stress in the film, which limits the yield for achieving $LiNbO_3$ thin-film on full wafer scale. In contrast, we use a wafer bonding and grinding process as shown in Fig. 1. We start with a Z-cut white $LiNbO_3$ wafer. The bonding surface is activated by plasma (similar to [15]). Then, the device wafer is flip-bonded to the Si handle wafer at room temperature. Therefore, the thermal stress is minimized, which allows us to achieve $LiNbO_3$ thin-film on full 4 inch wafer. The device wafer is then mechanically polished to 1um thickness.

To date, etching of $LiNbO_3$ have used either metal or silicon dioxide as a hard-mask, which increases the complexity and cause compatibility issues of the fabrication. In addition, any residue of metal left behind can interact with

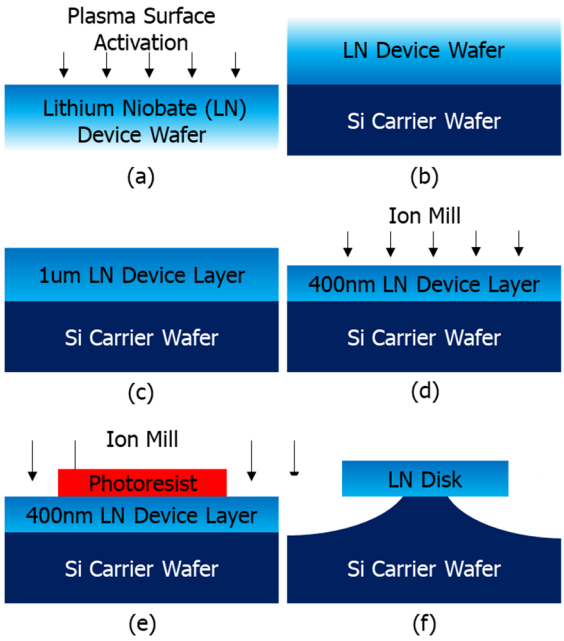

Fig. 1. Fabrication process of the LN disk optical resonator: (a) Prepare the device wafer for bonding by plasma surface activation; (b) Direct bonding of the LN device wafer to Si carrier wafer; (c) Grounding the device wafer to 1um thickness; (d) Ion mill with photoresist mask to define device geometry; (e) XeF2 timed-etch release.

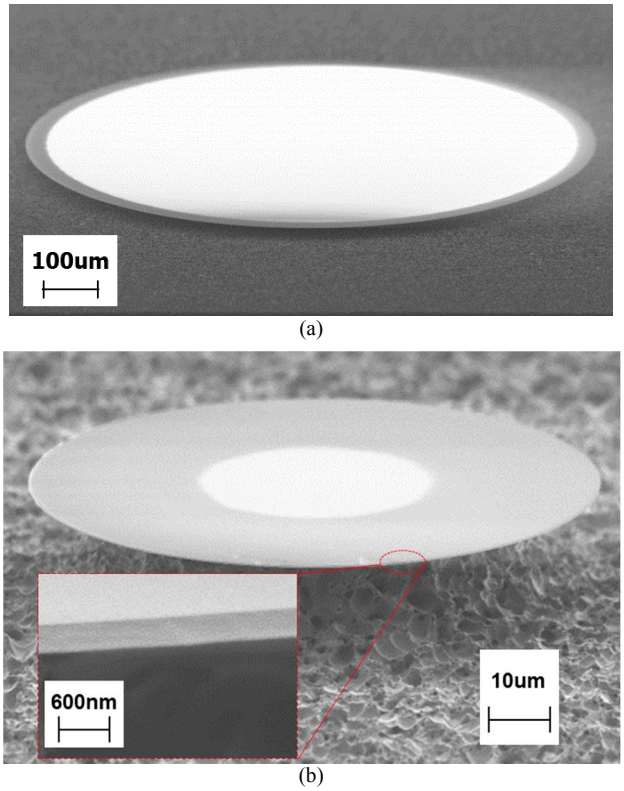

Fig. 2. (a) SEM of a 500um radius $LiNbO_3$ photonic disk resonator, (b) SEM of a 40um radius $LiNbO_3$ photonic disk resonator; Inset: Zoom-in view of the rim showing smooth side wall, which is crucial for high optical Q .

circulating photons causing optical absorption and scattering, which will significantly reduce the optical Q of the device. Here, we use 4um thick photo-resist as the mask with ion mill etching. The resist can then be easily rinsed off by acetone with sonication. If necessary, an additional O_2 plasma clean ensures that no residue is left behind. The argon ion mill etching can be controlled to be self-balancing between etching and re-sputtering by carefully adjusting the ion beam incident angle, where the re-sputtering can act as an extra sidewall protection during the etching [16]. With this process, we achieved sidewall angle of 87 degrees with <10nm surface roughness (inset of Fig. 2), thus enabling low scattering and meeting the requirement of a smooth vertical sidewall that is necessary for future integrated waveguide coupling. As the devices are intended to be characterized using a tapered optical fiber setup, a large refractive index mismatch exists between LN and SiO_2. Therefore, an extra blanket ion mill etching was performed to reduce the LN film thickness to ~400nm so that the optical modes in the thin film extends further into the air therefore reducing the effective mode index to match that in the tapered fiber.

Silicon has higher refractive index (~3.4) than LN (~2.3). So any light that couples into the niobate disk will leak into the silicon substrate. Using XeF_2 dry-etch to undercut the niobate disk resonator (Fig. 2) enables us to achieve >40um clearance between the niobate disk and silicon substrate, thereby enabling outstanding optical mode confinement in niobate and thus high optical Q. In addition, the free-standing disk structure will enable optomechanical [16] interactions between the mechanical and photonic modes.

III. Optical Measurements

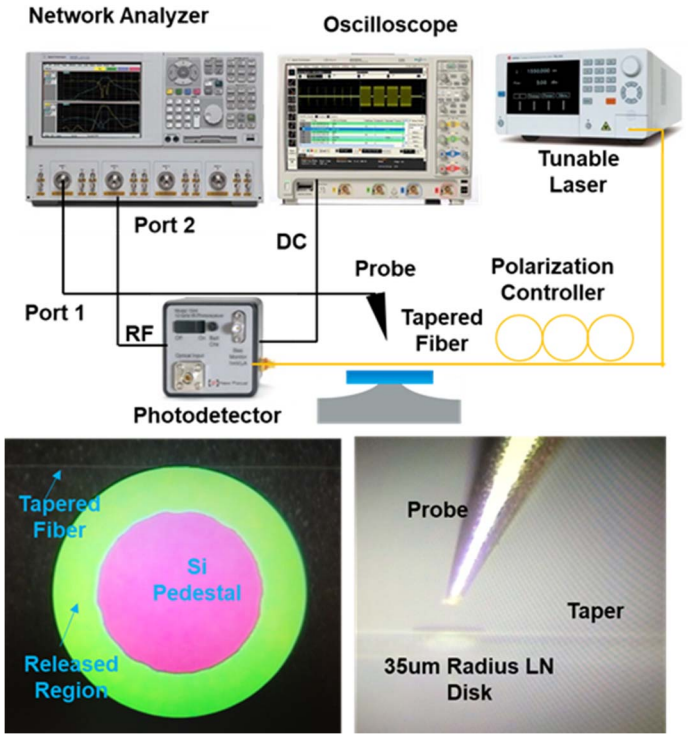

Fig. 3. Schematic of the characterization setup. Lower left inset: top view of the free-standing $LiNbO_3$ photonic disk resonator. Lower right inset: sideview of the acousto-optic modulation setup with a hovering probe to excite mechanical motion of the disk.

We use a tapered optical fiber [17] to couple light from a tunable near-IR laser (Santec TSL-510) to the niobate disk resonator (Fig. 3). A polarization controller is introduced to carefully adjust the light polarization in fiber such that it couples strongly with the photonic resonator. The transmitted optical signal is sent to a high-speed photodiode (Newport 1544A) and monitored on an Agilent (DSO9404A) oscilloscope. By sweeping the wavelength of the input light, we measure the optical transmission spectrum and extract the optical parameters (quality factor, group index, optical propagation loss) by fitting the transmission dip to a Lorentzian linewidth equation [17]. Fig. 4 shows the transmission spectrum of a 35um radius LN disk resonator from 1500nm to 1510nm. During the scan, the optical input power is kept below 20uW to ensure the heating of the resonator from the laser light does not cause asymmetric linewidth shape to interfere with the parameter extraction. One resonance at 1502.61nm is fitted to the Lorentzen linewidth equation, and the inset shows the zoom-in view (red curve). The extracted intrinsic optical Q is 484k, with a 95% confidence bounds from 458K to 509K, which is one of the highest demonstrated from thin-film LN devices.

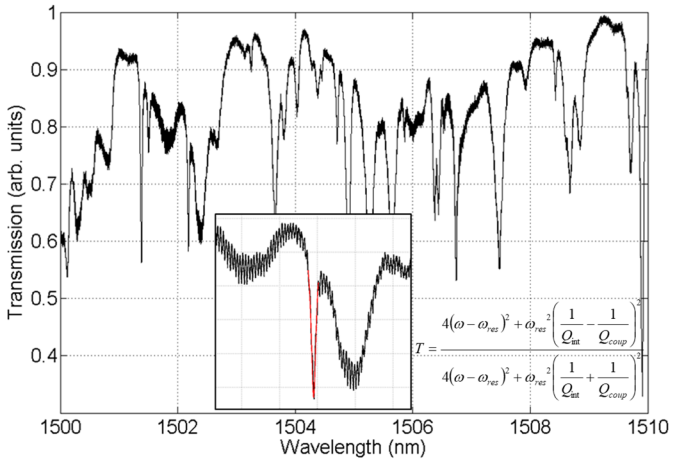

Fig. 4. Narrow band optical transmission spectrum of a 35um radius resonator, and curve fitting of one peak to a Lorentzen linewidth equation to extract the quality factor.

IV. Opto-mechanical Measurements

As the free-standing resonator body supports both mechanical and optical resonances, the optomechanical interaction can cause acousto-optic modulation of the transmitted light. The mechanical motion of the disk is excited by the piezoelectric effect and gradient force of electric field applied by a probe (Fig. 3). This causes effective optical path length change in the resonator causing the shift of the optical resonant frequency. When the wavelength of the input optical wave is biased at close to the 3dB transmission of the resonance, the frequency shift causes modulation of the transmitted optical power. Fig. 3 shows the schematic of the experimental setup. The probe is excited by supplying an AC voltage from port 1 of an Agilent (N5230A) network analyzer. The RF output of the photodetector is connected to port 2 of the network analyzer, while the DC output is monitored on the oscilloscope to track the transmitted DC optical power. The output power from port 1 of the VNA is 8dBm. Fig. 5 shows the broadband scattering parameter measurement from 300kHz to 2.5GHz. This allows us to identify various modes. Fig. 6 shows the zoom-in scattering parameter measurement result from 300kHz to 100MHz. The red curve shows the s-parameters noise floor without coupling the taper to the resonator, while the blue curve shows the s-parameters when the taper is coupled to the resonator and the input wavelength is biased at a high Q resonance around 1540nm. The wavelength is slowly tuned into the resonance from the short wavelength, and biased at the side of the resonance when the peaks in the S21 curve is maximized. The transmitted DC optical power is 70uW.

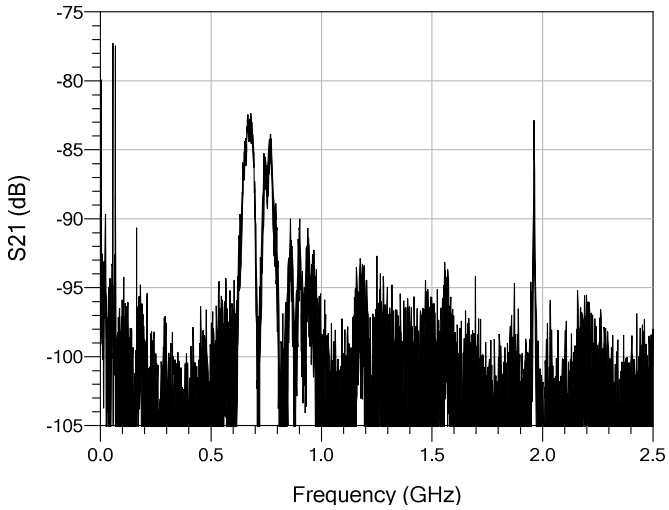

Fig. 5. Broadband scattering parameter measurement with the probe excitation.

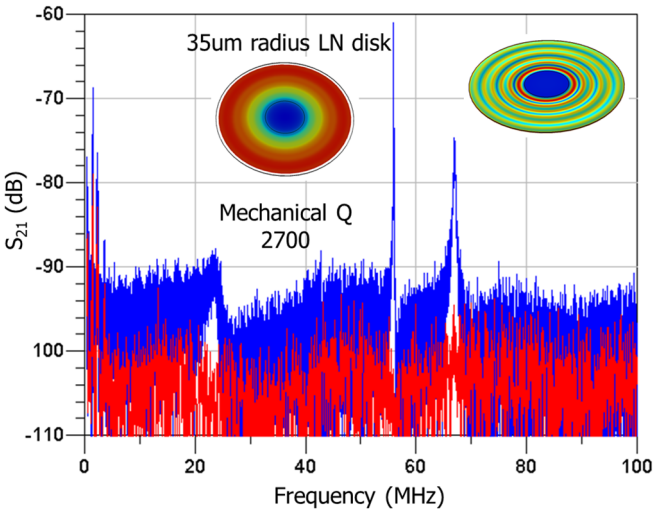

Fig. 6. Scattering parameter measurement with the probe excitation.

The S_{21} shows two peaks around 50MHz with very good signal to noise ratio. The peak at 56MHz in the S_{21} measurement corresponds to the radial breathing mechanical mode as shown in the figure, while the 67MHz peak corresponds to a radial shear mode. The mechanical Q of the breathing mode is 2700 by measuring the 3dB bandwidth of the peak. A 1.926GHz mechanical mode is also identified through the measurement (Fig. 7). In addition, a 15dBm single

tone RF signal at 56MHz was used to excite the breathing mode to generate acousto-optic modulation. The optical power in the generated side-band was 143nW when the DC optical power in the carrier is 70uW (Fig. 8).

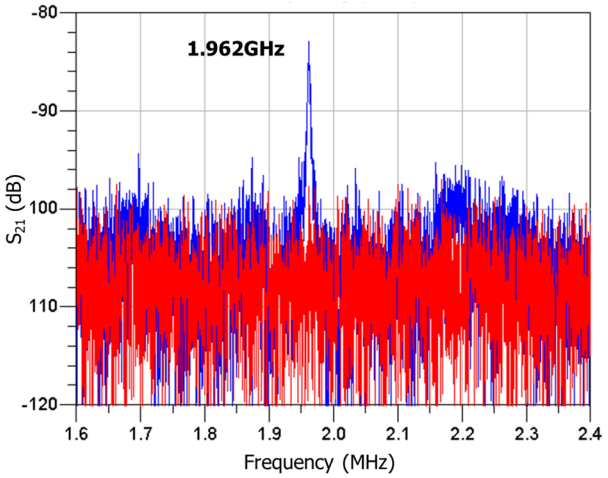

Fig. 7. Optomechanical modulation from a 1.962GHz mechanical mode.

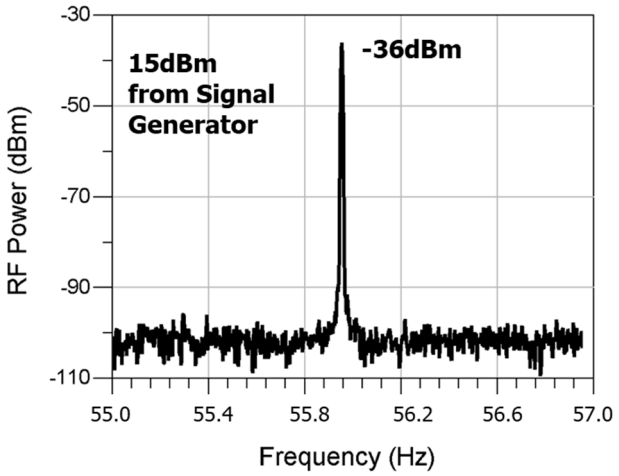

Fig. 8. Acousto-optical modulation through the 56MHz mechanical mode.

V. Conclusion

We have designed and demonstrated a micromachined Lithium Niobate optomechanical disk resonator. Using an external hovering RF probe, we can drive vibrations in the disk resonator at two bulk mode frequencies and achieve acousto-optic modulation. We also showed acousto-optical interaction up to ~1.9GHz, demonstrating that a center balanced minimal anchoring scheme has the potential to unleash the true limits of the niobate optomechanical platform. In conjunction with the intrinsic piezoelectric and electro-optic effects of $LiNbO_3$, optomechanical interactions can enhance and enable many novel thin film lithium niobate photonic devices [19].

VI. Acknowledgement

This work was performed in part at the Cornell NanoScale Facility, a member of the National Nanotechnology Coordinated Infrastructure (NNCI), which is supported by the National Science Foundation (Grant NNCI-1542081).

VII. References

[1] R. S. Weis and T. K. Gaylord, “Lithium niobate: Summary of physical properties and crystal structure,” Appl. Phys. A. 37(4), pp. 191–203, 1985.

[2] R. Wang and S. A. Bhave, "High Optical Q, GHz FSR Lithium Niobate-on-silicon photonic resonators," 2014 Solid State Sensor, Actuator and Microsystems Workshop (Hilton Head 2014), Hilton Head Island, South Carolina, June 8-12, 2014.

[3] C. Wang, M. Zhang, X. Chen, M. Bertrand, A. Shams-Ansari, S. Chandrasekhar, P. Winzer, and M. Loncar, “Integrated lithium niobate electro-optic modulators operating at CMOS-compatible voltages,” Nature 562, pp. 101–104, 2018.

[4] C. Wang, M. Zhang, M. Yu, M., R. Zhu, H. Hu, and M. Loncar, “Monolithic lithium niobate photonic circuits for Kerr frequency comb generation and modulation,” Nat. Commun. 10, 978, 2019.

[5] M. Mahmoud, A. Mahmoud, L. Cai, M. Khan, T. Mukherjee, J. Bain, and G. Piazza, "Novel on chip rotation detection based on the acousto-optic effect in surface acoustic wave gyroscopes," Opt. Express 26, pp. 25060-25075, 2018.

[6] L. Shao, M. Yu, S. Maity, N. Sinclair, L. Zheng, C. Chia, A. Shams-Ansari, C. Wang, M. Zhang, K. Lai, and M. Lončar, "Microwave-to-optical conversion using lithium niobate thin-film acoustic resonators," Optica 6, pp. 1498-1505, 2019.

[7] W. Jiang, R. N. Patel, F. M. Mayor, T. P. McKenna, P. Arrangoiz-Arriola, C. J. Sarabalis, J. D. Witmer, R. Van Laer, and A. H. Safavi-Naeini, "Lithium niobate piezo-optomechanical crystals," Optica 6, pp. 845-853, 2019.

[8] G. Nunzi Conti, S. Berneschi, F. Cosi, S. Pelli, S. Soria, G. C. Righini, M. Dispenza, and A. Secchi, “Planar coupling to high-Q lithium niobate disk resonators,” Opt. Express 19(4), pp. 3651–3656, 2011.

[9] L. Zhou and A. W. Poon, “Silicon electro-optic modulators using p-i-n diodes embedded 10-micron-diameter microdisk resonators,” Opt. Express 14(15), pp. 6851-6857, 2006.

[10] H. L. R. Lira, C. B. Poitras, and M. Lipson, “CMOS compatible reconfigurable filter for high bandwidth nonblocking operation,” Opt. Express 19(21), pp. 20115-20121, 2011.

[11] J. C. Hulme, J. K. Doylend, and J. E. Bowers, “Widely tunable Vernier ring laser on hybrid silicon,” Opt. Express 21(17), pp. 19718-19722, 2013.

[12] T.Wang, J. He, C. Lee, and H. Niu, “High-quality LiNbO3 microdisk resonators by undercut etching and surface tension reshaping,” Opt. Express 20(27), pp. 28119–28127, 2012.

[13] R. Wang, S. A. Bhave and K. Bhattacharjee, "Design and Fabrication of S0 Lamb-Wave Thin-Film Lithium Niobate Micromechanical Resonators," in Journal of Microelectromechanical Systems, vol. 24, no. 2, pp. 300-308, April 2015.

[14] A. Guarino, G. Poberaj, D. Rezzonico, R. Degl’Innocenti, and P. Gnter, “Electro-optically tunable microring resonators in lithium niobate,” Nature Photonics 1, pp. 407-410, 2007.

[15] D. Tulli, D. Janner, and V. Pruneri, “Room temperature direct bonding of LiNbO3 crystal layers and its application to high-voltage optical sensing,” J. Micromech. Microeng. 21(8), 2011.

[16] R. Wang, S. A. Bhave, and K. Bhattacharjee, “Thin-film high $k_t^2 \times Q$ multi-frequency lithhium niobate resonators,” 26th IEEE International Conference on MEMS, pp. 165–168, 2013.

[17] T. J. Kippenberg and K. J. Vahala, “Cavity optomechanics: back-action at the mesoscale,” Science 321(5893), pp. 1172–1176, 2008.

[18] M. Cai, O. Painter, and K. J. Vahala, “Observation of critical coupling in a fiber taper to a silica-microsphere whispering-gallery mode system,” Phys. Rev. Lett. 85(1), pp. 74–77, 2000.

[19] A. Honardoost, K. Abdelsalam, and S. Fathpour, “Rejuvenating a versatile photonic material: thin-film lithium niobate,” Laser & Photonics Reviews 2000088, 2020.